Wind Turbine Design Using Thin Airfoil SD2030

Takeyeldein, M. M.
Department of Aeronautical, Automotive, and Ocean Engineering, School of Mechanical Engineering, Faculty of Engineering, Universiti Teknologi Malaysia

Lazim, Tholudin Mat
Department of Aeronautical, Automotive, and Ocean Engineering, School of Mechanical Engineering, Faculty of Engineering, Universiti Teknologi Malaysia

Nik Mohd, N.A.R
Department of Aeronautical, Automotive, and Ocean Engineering, School of Mechanical Engineering, Faculty of Engineering, Universiti Teknologi Malaysia

Ishak, Iskandar Shah
Department of Aeronautical, Automotive, and Ocean Engineering, School of Mechanical Engineering, Faculty of Engineering, Universiti Teknologi Malaysia

他

Wind Turbine Design Using Thin Airfoil SD2030

M. M. Takeyeldein[1], Tholudin Mat Lazim[1,*], Nik Mohd, N.A.R[1], Iskandar Shah Ishak[1], Essam Abubakr Ali[1]

[1]Department of Aeronautical, Automotive, and Ocean Engineering, School of Mechanical Engineering, Faculty of Engineering, Universiti Teknologi Malaysia, Malaysia

*Author to whom correspondence should be addressed,
E-mail: tholudin@fkm.utm.my

This paper presents the performance of a horizontal axis wind turbine of diameter 0.6 m designed to operate at low Reynolds number. In this design work, the SD2030 thin airfoil was selected as a profile section for the turbine blades. The taper ratio, section twist angle and blade angle were optimized using the Blade Element Momentum (BEM) theory. In a numerical investigation, the aerodynamic flow field was computed using the two-dimensional Reynolds Averaged Navier-Stokes equations for incompressible flow to predict the performance of the airfoil at the Reynolds number of 1×10^5. The numerical results obtained were in accordance with the wind tunnel test's result and thus validating this Computational Fluid Dynamics (CFD) works. Results depict that this new turbine design with the airfoil of SD2030 can rotate at a low start-up wind speed of 2.4 m/s, testifying that the design is successful, and that the turbine is capable to operate at low Reynolds number such as 1×10^5 with the desired output.

Keywords: Low Reynolds Number Airfoil, Wind Turbine Aerodynamics, CFD, Wind Tunnel Test.

1. Introduction

The aerodynamics of wind turbine operating at low wind speed is challenging because of the laminar separation that happens at low Reynolds number. Flow around an airfoil at low Reynolds number below 5×10^5 might separate while the boundary layer is still laminar and before the transition to turbulent. This laminar separation might result into forming air bubbles known as the laminar separation bubbles, which cause extra drag to the airfoil and is defined by the bubble drag. Figure 1 shows a general structure of laminar separation bubbles. A typical airfoil not designed for a low Re regime will suffer a loss in performance. Many thin airfoils were designed to operate at low Re and reduce the effect of the separation bubble, such as E387 and SD2030 airfoils[1,2].
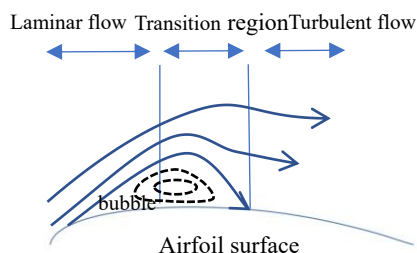

Laminar flow Transition region Turbulent flow

bubble

Airfoil surface

Fig. 1: A general structure of a laminar separation bubble[1)]

The objectives of this study are:

- To choose an airfoil that is suitable for wind turbine operating at low Reynolds number.
- To perform a two-dimensional CFD analysis of the chosen airfoil at Reynolds number of 1×10^5 using three different turbulence models, Shear-Stress Transport (SST) k-ω, k-kl-ω transition model, and transition SST model; this is to find which one can predict the most accurate, the aerodynamics of the airfoil during the laminar separation.
- To design a low Reynolds number wind turbine and find its performance using Blade Element Momentum (BEM).
- to find the start up speed and maximum RPM of the new wind turbine, at three different pitch angles, using wind tunnel tests.

2. Airfoils for wind turbines

Wind turbine blades are responsible for converting the wind power into mechanical power. The modern wind turbine blades, have an airfoil shape as a cross-section, which makes the choice of the airfoil of a great significance to the wind turbine design[3).]The common

early choices of airfoils for horizontal wind turbines were aircraft airfoils designed for aviation, such as NACA four-digit series NACA 44-XX, NACA five-digit series NACA 230xx, NACA six digits series like NACA 632-XX, and NASA LS (1) MOD [3,4]. Despite that, some of these airfoils got a high maximum lift and low minimum drag, however they were designed to operate at Reynolds number higher than that in wind turbines, which might influence the performance of turbines because of their sensitivity to surface roughness[3,4]. Later, many airfoils have been designed for wind turbines applications, that took into consideration design criteria like achieving maximum lift that is insensitive to surface roughness and producing a smooth stall. As an example of the most commonly used airfoils currently are RISO-airfoils, DU-airfoils, S-Series airfoils, and FFA [3–6]. The MEXICO experimental wind turbine as an example, uses three different airfoil series at different stages of its blade, it uses, DU91-W2-250, RISO A1-21 and NACA 64-418 airfoils [7].

3. Airfoils for wind turbines at low Reynolds number

As mentioned earlier there are airfoils designed and tested for low Reynolds number flow regimes applications, some of them were intended to be used for wind turbines and others for other applications such as sail planes or UAV. An example of low Re airfoils is, S1210, S1221, S1223, SH3055, FX-631 37, E387, SG6043, SG6040, SG6041, SG6042, Aquila, S822, SD2030, S834, NACA 632xx, and NACA 4418 [8–13].

These airfoils have something in common, they have a gradual transition ramp on the upper surface; so, to increase the camber of the airfoil and hence the aerodynamic loads; the trailing edge would be cusped as shown in Figure 2 with S1223 airfoils which is known as a high lift low Re airfoil.
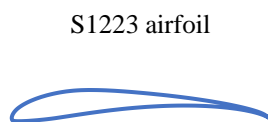
S1223 airfoil

Fig. 2: S1223 airfoil, is a high lift low Reynolds number airfoil, with a highly cusped trailing edge [11].

The cusped trailing edge could make the manufacturing of the turbine challenging because of its weak structure, so airfoils with high cusped trailing edge are excluded from being a choice. The least cusped thin airfoils are

listed in Table 1 and shown in Figure 3.

**Table 1:** Low Reynolds number airfoils with low cusped tailing edge.

The airfoil	Thickness	Camber
E387	9.07%	3.78%
SD2030	8.56%	2.23%
SG6041	10%	2%
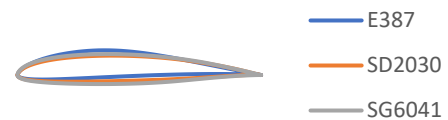
Fig. 3: The three airfoils listed in Table 1 [9,10]. (a) SD2030. (b) SG6040. (c) E387.

By comparing the drag polar curve of those three airfoils as shown in Figure 4, the SD2030 is chosen to be used for the following arguments:

- It has a lower minimum drag at low Reynolds number 1×10^5.
- It has a wider drag bucket which shows that its high L/D happens over a wider range of angles of attack.
- The drag knee happens at a lower (peak drag) than E387 and SG6041 [9,10]. [At a low Reynolds number at a certain angle of attack the drag spikes because of the formation of separation bubbles, known as the drag knee.]
- It has been used before in two commercial wind turbines; Southwest AirX And Air403[9].
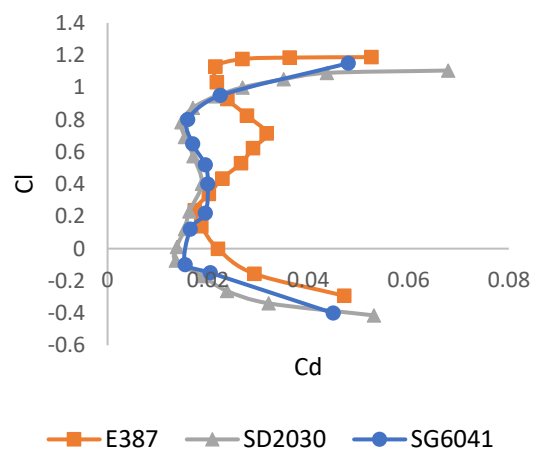
Fig. 4: The drag knee at Re=1x 105 happened in the case of SD2030 at a lower peak drag (Cd <0.02) [9,10].

4. 2D CFD simulation of SD2030 airfoil.

The air flow around SD2030 airfoil is simulated at Reynolds number 1×10^5, using the Reynolds averaged Navier-stokes equations for incompressible flow. The main objective of this section is to examine three turbulence models which are, (SST) k-ω, k-kl-ω, and Transition SST, at such low Reynold number and validate the results with wind tunnel testing results. These three turbulence models were selected based on the studies conducted by Zidane et al[14], and Aftab et al[15]. The continuity and momentum equation resulting from Reynolds averaged Navier-stokes equations are as follows:

$$\frac{\partial(\bar{u}_i)}{\partial x_i} = 0 \qquad (1)$$

$$\frac{\partial(\bar{u}_i)}{\partial t} + \frac{\partial}{\partial x}\left(\bar{u}_i \bar{u}_j\right) = -\frac{1}{\rho}\frac{\partial \bar{p}}{\partial x_i} + \nu \frac{\partial^2 \bar{u}_i}{\partial x_i \partial x_j} + \frac{\partial \tau_{ij}}{\partial x_j} \qquad (2)$$

Where:

$\bar{u}$=Velocity Vector
x=displacement vector
t=time
$\bar{p}$=pressure
ν =Kinematic viscosity
τ_{ij}=Reynolds stress tensor
*The over bar indicates a time-averaged quantity.

### 1. Model description and Grid convergence study

The computational domain with the boundary conditions used during the simulation process is shown in Figure 5 (a), which had been divided into two zones as shown in Figure 5 (b) and Figure 5 (c), respectively. The first zone which has a C-shape is located near to the wall of the airfoil, the mesh in this zone is structured and the layer height close to the wall is chosen to make sure Y plus is less than 1, to capture the boundary layer, flow separation and reattachments; similar to what was followed by Amr et al.[16], Hakim et al. [17], and Mohd NARN et al[18], this zone was constructed using Ansys ICEM CFD software. The second zone which represents the far field, is meshed into unstructured triangular element, and it was constructed using Ansys meshing.
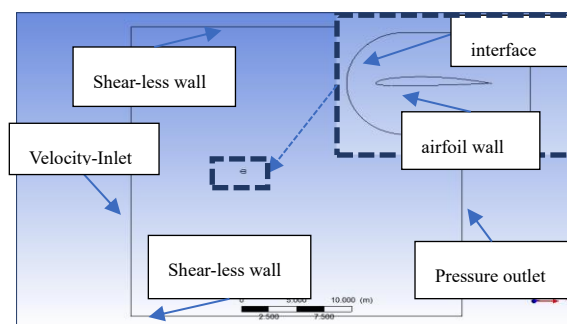
(a)
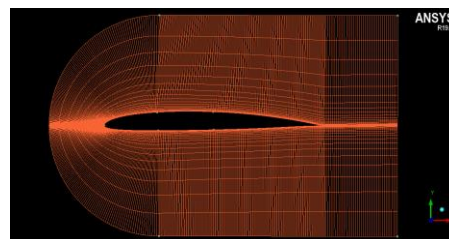
(b)
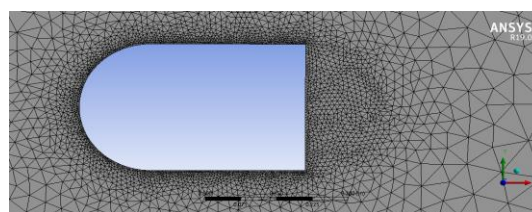
(c)

Fig. 5: (a) Computational zone and Boundary conditions. b) First zone: C-mesh around the airfoil. (c) Second Zone: unstructured triangular mesh elements in the far field.

Before running the final simulation, grid independence analysis was carried out to verify that the results obtained are free from grid influence[13–15,19]. This was done by increasing the number of nodes along the airfoil parallel to the flow direction, then by changing the first layer height while fixing the growth rate; to make sure the Y plus at the airfoil surface is less than one, and last by increasing the number of layers normal direction in the C-grid while fixing the first layer height chosen in step 2 as shown in Figure 6 and Table 2. The final grid used is, 200 nodes in the flow direction, 110 layers in the normal direction with exponential growth rate 1.1, and the Y plus in the first layer elements is 0.1.

Table 2: Grid convergence study for the drag coefficient at different mesh settings.

$Cd_{0.11°}$	N_p	$Cd_{0.11°}$	Y_{plus}	$Cd_{0.11}$	GR	N_n
0.014962	100	0.01509	0.01	0.014932	1.7	25
0.01504	116	0.015143	0.1	0.015143	1.46	32
0.01511	150	0.015166	1	0.014848	1.2	62

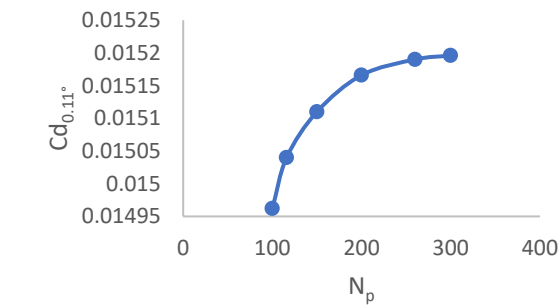| 0.015166	200	0.015118	2	0.014679	1.1	110
0.01519	260	0.015127	5	0.014639	1.05	180
0.015196	300					

Where:

$Cd_{0.11°}$=drag coefficient at AOA 0.11°
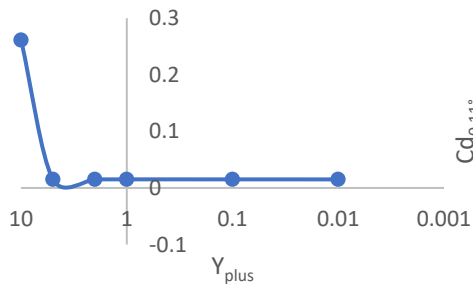
N_p= No of nodes in the direction of airfoil surface

Y_{plus}= Y plus at the first layer normal to the surface

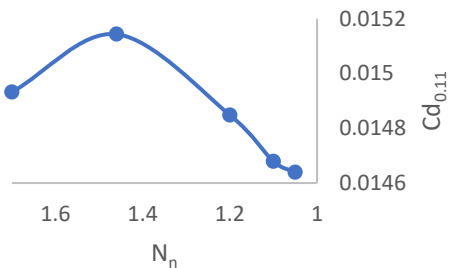GR=Growth rate of the distance between the normal layers to the surface

N_n= No. of layers normal to the airfoil surface (Nn)

(a)

(b)

(c)

Fig. 6: Convergence of the Cd value at different mesh settings. (a) no. of node points vs CD (b) Yplus vs Cd (c) Growth rate of normal layers vs CD

CFD Results and Validation

This section presents a comparison made between those three turbulence models, with the wind tunnel test results and Xfoil, to determine which model is more accurate in predicting the flow phenomena at low Reynolds number. Figure7 and Figure8 shows the drag and lift curves of the airfoil. It is shown from the lift curve of the experimental results illustrated in Figure 9 that the drag knees happened at angle of attack, AOA= 2.17°, and hence the corresponding values of Cl and Cd are tabulated in Table3 for further discussion. The turbulence model (SST) k-ω is the more accurate in predicting the drag coefficient, and k-kl-ω is the best in predicting the lift coefficient. It is also noticeable that, transition SST model underestimate the drag while overestimating the lift, k-kl-ω model do the vice versa to transition SST model, while (SST) k-ω underestimate both coefficients.
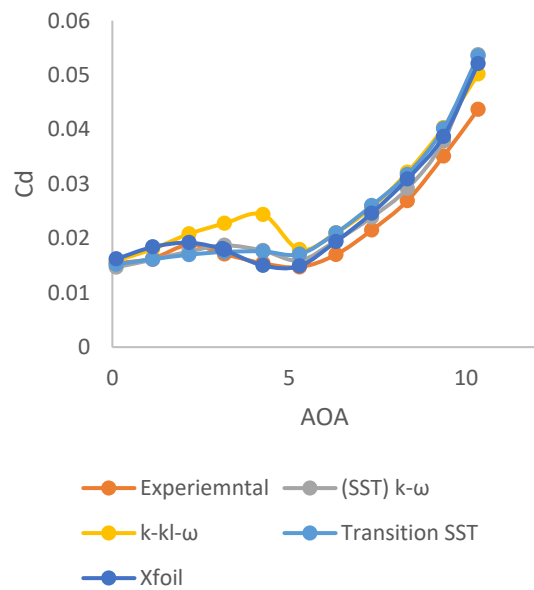
Fig. 7: Drag curve of SD2030 airfoil evaluated by different turbulence models, Xfoil, and wind tunnel test.
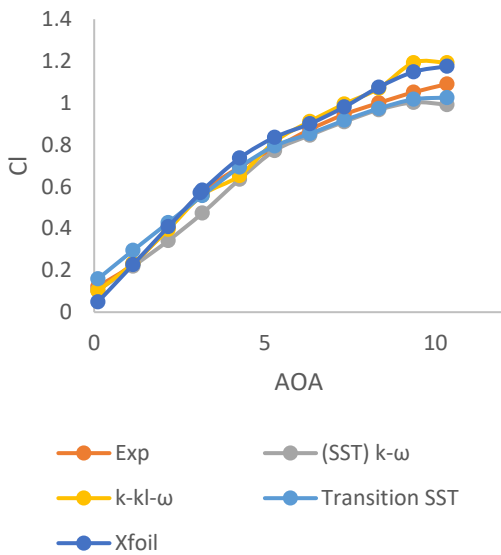
Fig. 8: Lift curve of SD2030 airfoil evaluated by different turbulence models, Xfoil, and wind tunnel test.
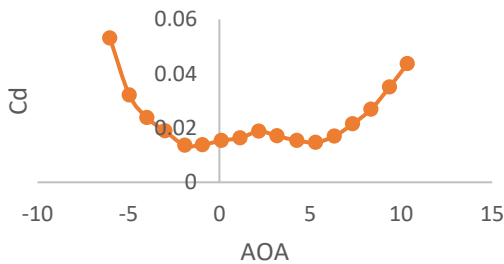

**Fig. 9:** Drag polar of sd2030 airfoil evaluated by wind tunnel test [9].

Table 3: Cl and Cd values at AOA 2.17 ° evaluated by different methods.

| Method	Cl	Cd
Wind tunnel	0.403	0.0188
Xfoil	0.4085	0.0192
SST	0.34192	0.017586
K Kl	0.39538	0.020805
SST 4eqns	0.42766	0.016984

Velocity contours of the flow around the airfoil at AOA 2.17° is shown in Figure 10. the contours show that flow separates at early stage from the surface of the airfoil and doesn't reattach again, which agrees with the literature that flow separated while the flow is laminar may or may not reattach again [1].
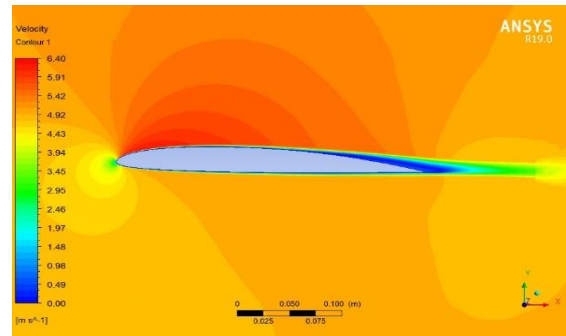
(a)
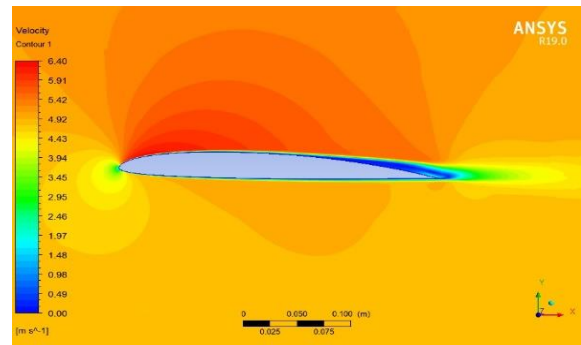
(b)
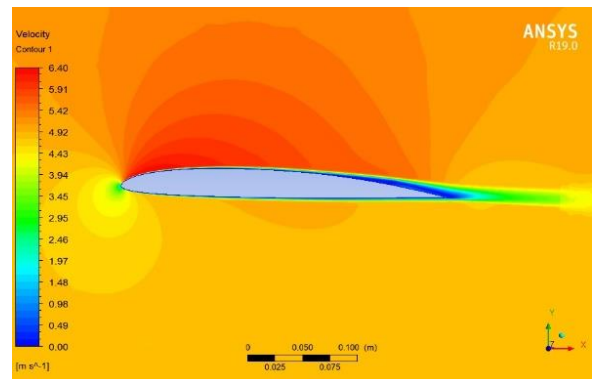
(c)

Fig. 10: Velocity contour around SD2030 airfoil at AOA 2.17° evaluated by three different turbulence models (a) (SST) k-ω (b) k-kl-ω (c) Transition SST

5. Wind turbine design

The objective of this research work is to design a three bladed wind turbine model with thin airfoil section SD2030 that can start rotation at a small start-up speed; less than 3m/s.
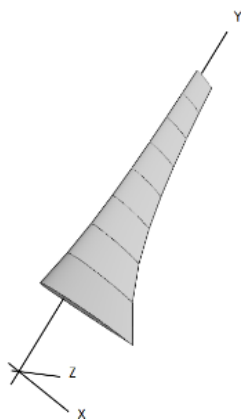
Initial design

BEM theory have been recognized as a design and optimization tool for wind turbines[20]. The twist angle of the blade is optimized to have an angle of attack angle of 5° at the design point; and hence it is called the design

angle of attack; this the same angle at which Cl/Cd max of SD2030 airfoil happens at Reynolds number 5×10^5. A resulted sectional pitch angle difference of 20° between the tip and the root, make it easier for starting up. The blade chord distribution was optimized using Schmitz which is based on Betz limit optimization, however, it results in a smaller chord size at the root [21]. Table 4 shows the twist and taper distribution of the blade. Figure 11 shows the performance of the initial blade design calculated using BEM, it is shown that the maximum Power Coefficient Cp happens at a tip speed ratio TSR= 5.5.

Table 4: Geometry parameters of the initial rotor design.

| Section Position(m)	Chord length (m)	Twist angle °
0.06	0.08	20.02
0.09	0.06	12.17
0.12	0.05	7.95
0.15	0.04	5.34
0.18	0.03	3.58
0.21	0.03	2.31
0.24	0.03	1.35
0.27	0.02	0.60
0.3	0.02	0.00

(a)
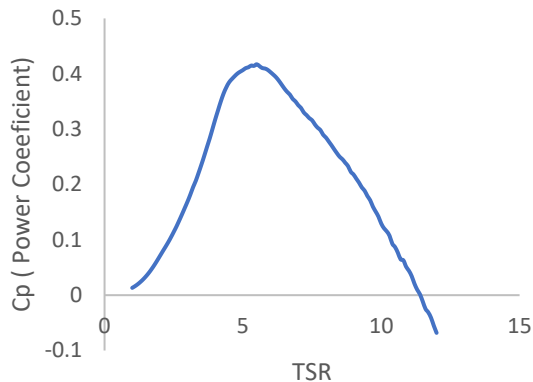
(b)

Fig. 11: (a) initial rotor model (b) Cp-TSR curve of the initial rotor calculated using BEM (Qblade)

The final design

The criteria of the design shown in the previous section meets the objectives; however, a modification was applied to thicken chord distribution for two reasons:

- To have a better start up speed (lower start-up speed), based on the conclusion of the study done by Hsiao et al. [13] that shows that un-tapered blade (thicker chord) shifted the power curve to operate at lower Tip-Speed-Ratio. (TSR) range than the tapered one (thinner chord).
- To have a stronger blade structure, especially because only one type of airfoil is used (no special airfoil used for the root part).

Figure 12 shows the difference in the torque between the first turbine and second turbine, the second turbine has a higher torque value at low tip speeds ratio (TSR<5) and hence the turbine will have a better starting up. The chord and twist distribution of the final blade are shown in Table 5 and Figure 13 a. The power coefficient curve is shown in Figure 13 b, the maximum power coefficient is 0.414 and it happens at TSR= 4.3.
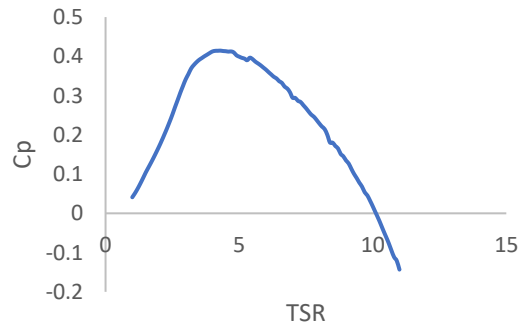
Torque vs TSR
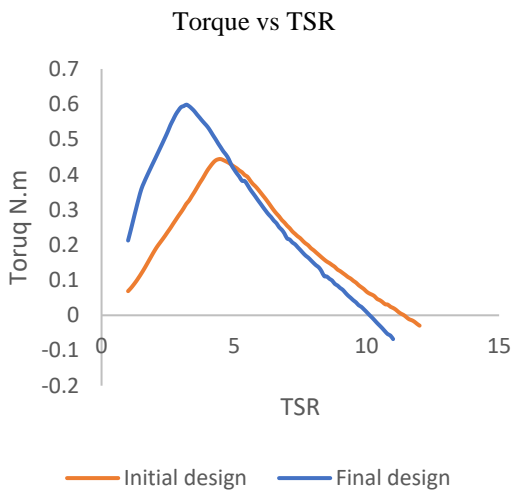
Fig. 12: A comparison between the Torque-TSR curves of the initial and final rotor designs

Table 5: Geometry parameters of the final rotor design.

| Position (m)	Chord (m)	Twist (°)
0.06	0.09	20
0.09	0.0825	12.2
0.12	0.075	8
0.15	0.0675	5.3
0.18	0.06	3.6
0.21	0.0525	2.3
0.24	0.045	1.3
0.27	0.0375	0.6
0.3	0.03	0
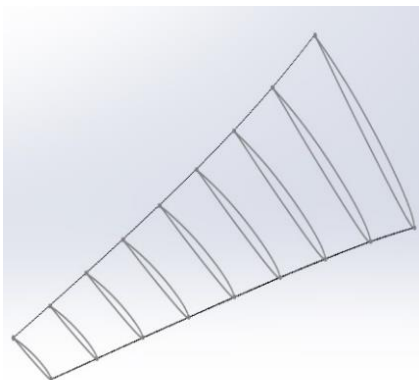
(a)

(b)

Fig. 13: (a) Final rotor model (b) Cp-TSR curve of the final rotor calculated using BEM (Qblade)

The final turbine description is shown in Table 6. The distribution, of the Reynolds number, and the angles of attack along the blade radial position are shown Figure 14, which were calculated at TSR which gives maximum Cp. It is shown that Reynolds number range is between 7×10^4 and 1×10^5, and the angle of attack range in all sections is all in the attaching region.
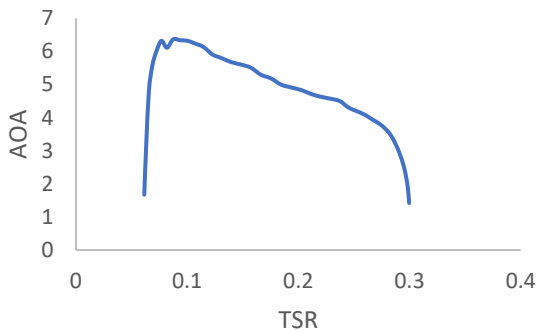
Table 6: Turbine description.

Number of blades	3
Radius	0.3 m (0.24m blade+0.06 hub)
Airfoil	SD2030
CP max	0.414
TSR @ Cp_{max}	4.3
Rated speed	10 m/s
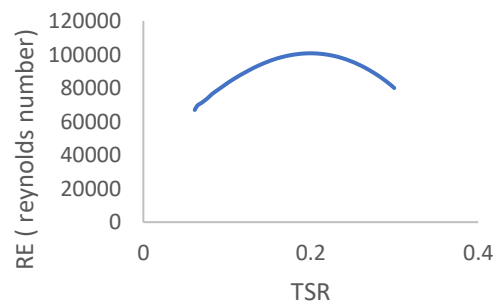
(a)

(b)

(a)

Fig. 14: (a) Reynolds number along the radial position at TSR=4.3. (b) AOA along the radial position at TSR=4.3.

6. Wind tunnel testing

Experimental works have been recognized as a well-testified instrumentation to conduct the research[22–25]. Hence, the turbine model of the final design had been fabricated to be tested at the Universiti Teknologi Malaysia's wind tunnel (UTM-LST). UTM-LST as shown in the schematic in Figure 15 (a) is a closed-circuit tunnel with the dimension of the test section is 1.5m (H) × 2.0m(W) × 6m(L) and the maximum wind speed of 80 m/s [26].

The main objective of the test was investigating the start-up speed of the turbine at different pitch angles; three different pitch angles 3°,5° &7° were examined, the pitch angle 7° has shown the least start-up speed at just 2.4 m/s. The change of the maximum RPM of the turbine at each pitch angle, with the change of the upwind speed is also investigated during the test.

During the test set-up, a laser light device was used to center the wind turbine (Figure 15 c) to ensure a precise alignment of the turbine to the upcoming wind. The desired pitch angles were set using an electronic inclinometer. The start up speed were monitored using the wind tunnel speed measurement system once the turbine rotates. Finally, after the turbine reached the maximum rotational speed, the RPM of the turbine was measured during the test using a tachometer device.


(b)

(c)

Fig. 15: The wind turbine model is fixed in the testing section of UTM LST wind tunnel.

Figure 16 shows the maximum RPM of the turbine at different upwind speed for each of the three pitch angles measured by a tachometer in the wind tunnel. since there is no resisting toque applied to the turbine, it can be noticed that the rotating speed is increasing directly proportional with the wind tunnel upwind speed. Also, it can be noticed that at angle 7° the turbine start-up speed is the lowest, but this high pitch angle has an inverse effect

at higher TSR, it can be concluded from the graph in Figure 16 that the TSR range of operation is the narrowest at this pitch angle.
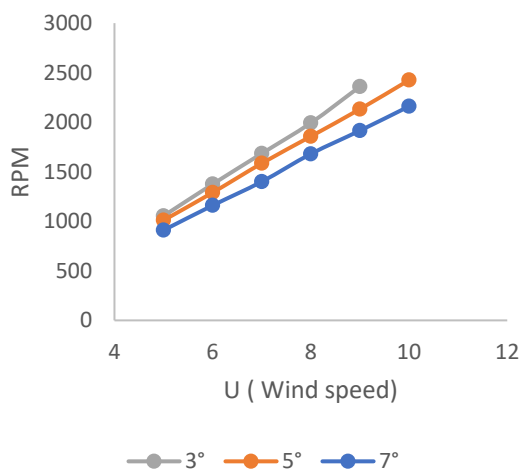
Fig. 16: RPM of the turbine during the wind tunnel test

7.   Conclusion

This research had designed a horizontal axis wind turbine that could rotate at a low start up wind speed of 2.4 m/s. The selection of the thin airfoil SD2030 for this turbine had been proven to be a wise decision as the turbine can operate at low Reynolds number of 1×10^5. This testifies that SD2030 is a good airfoil for a small low Reynolds number wind turbine. The final modification made to thicken the blade had increased the torque up to almost 100% at low TSR which, make the turbine has a better start-up speed.

Acknowledgements

References

1) D. Mclean, "Understanding Aerodynamics: Arguing from the Real Physics," Wiley-Blackwell, (2013).

2) P. Giguere, and M.S. Selig, "Low reynolds number airfoils for small horizontal axis wind thrbines," Wind Eng., 21 (6) 367–380 (1997).

3) J.F. Manwell, J.G. McGowan, and A.L. Rogers, "Wind energy explained," Wind Eng., vii, 577 p. (2002).

4) J. Tangler, and D. Somers, "NREL airfoil families for hawts," Awea, (1) 1–12 (1995).

5) F. Bertagnolio, and N. Sorensen, "Wind turbine airfoil catalogue," Risø-R-1280 (EN), Risø …, (2001).

6) P.J. Schubel, and R.J. Crossley, "Wind turbine blade design," Energies, 5 (9) 3425–3449 (2012).

7) H. Snel, J.G. Schepers, and B. Montgomerie, "The mexico project (model experiments in controlled conditions): the database and first results of data processing and interpretation," J. Phys. Conf. Ser., 75 012014 (2007).

8) R.K. Singh, M.R. Ahmed, M.A. Zullah, and Y.-H. Lee, "Design of a low reynolds number airfoil for small horizontal axis wind turbines," Renew. Energy, (2011).

9) M.S. Selig, and B.D. McGranahan, "Wind tunnel aerodynamic tests of six airfoils for use on small wind turbines," J. Sol. Energy Eng., 126 (4) 986 (2004).

10) P. Giguère, and M.S. Selig, "New airfoils for small horizontal axis wind turbines," J. Sol. Energy Eng., 120 (2) 108 (1998).

11) M.S. Selig, and J.J. Guglielmo, "High-lift low reynolds number airfoil design," J. Aircr., 34 (1) 72–79 (1997).

12) Y. Ohya, T. Karasudani, A. Sakurai, K. ichi Abe, and M. Inoue, "Development of a shrouded wind turbine with a flanged diffuser," J. Wind Eng. Ind. Aerodyn., 96 (5) 524–539 (2008).

13) F. Hsiao, C. Bai, and W. Chong, "The performance test of three different horizontal axis wind turbine (hawt) blade shapes using experimental and numerical methods," Energies, 6 (6) 2784–2803 (2013).

14) I.F. Zidane, G. Swadener, K.M. Saqr, X. Ma, and F. Mohamed, "CFD Investigation of Transitional Separation Bubble Characteristics on NACA 63415 Airfoil at Low Reynolds Numbers," in: Proc. 25th UKACM Conf. Comput. Mech., (2017).

15) S.M.A. Aftab, A.S.M. Rafie, N.A. Razak, and K.A. Ahmad, "Turbulence model selection for low reynolds number flows," PLoS One, 11 (4) e0153755 (2016).

16) A.M. Halawa, B. Elhadidi, and S. Yoshida, "Aerodynamic performance enhancement using active flow control on DU96-W-180 wind turbine airfoil," Evergreen, 5 (1) 16–24 (2018).

17) A.H.A. Rahman, N.A.R.N. Mohd, T.M. Lazim, and S. Mansor, "Aerodynamics of harmonically oscillating aerofoil at low reynolds number," J. Aerosp. Technol. Manag., 9 (1) 83–90 (2017).

18) N.A.R.N. Mohd, and G. Barakos, "Performance and wake analysis of rotors in axial flight using computational fluid dynamics," 9 193–202 (2017).

19) I.S. Ishak, S. Mansor, T. Mat Lazim, and M.R. Abd Rahman, "Numerical studies on unsteady helicopter main-rotor-hub assembly wake," J. Adv. Res. Fluid Mech. Therm. Sci., 1 (1) 190–200 (2018).

20) E.A. Efkirn, T.M. Lazim, W.Z.W. Omar, N.A.R.N. Mohd, and M.M. Takeyeldein, "Aerodynamic Analysis of Horizontal Axis Wind Turbine Using Blade Element Momentum Theory for Low Wind Speed Conditions," in: (2015): pp. 12–16.

21) D. Marten, and J. Wendler, "QBlade guidelines," (2013).

22) I.S. Ishak, and Z.M.F. Mougamadou, "Effects of helicopter horizontal tail configurations on aerodynamic drag characteristics," J. Teknol., 4 67–72 (2017).

23) K.A. Kasim, S. Mat, I.S. Ishak, and M. Said, "Effects of propeller locations on the vortex system above delta-shaped uav model," 30th Congr. Int. Counc. Aeronaut. Sci. ICAS 2016, (2016).

24) O.M.A.M. Ibrahim, and S. Yoshida, "Experimental and numerical studies of a horizontal axis wind turbine performance over a steep 2d hill," Evergreen, 5 (3) 12–21 (2018).

25) I.S. Ishak, N.A.R.N. Mohd, and S. Mat, "Aerodynamic study of air flow over a curved fin rocket akademia baru journal of advanced research in fluid aerodynamic study of air flow over a curved fin rocket," (2017).

26) S. Wiriadidjaja, F. Hasim, S. Mansor, W. Asrar, A.S.M. Rafie, and E.J. Abdullah, "Subsonic wind tunnels in malaysia: a review," Appl. Mech. Mater., 225 566–571 (2012).